SOUND PROPAGATION OVER PERIODIC ROUGHNESS

K Attenborough Engineering and Innovation, The Open University, Milton Keynes, UK
S Mellish Engineering and Innovation, The Open University, Milton Keynes, UK
S Taherzadeh Engineering and Innovation, The Open University, Milton Keynes, UK
I Bashir Electronic and Computer Engineering, Teeside University, Middlesborough, UK
A Stronach RPS Group, Manchester, UK

1 INTRODUCTION

Sound propagating from a point source in air over a rough acoustically hard boundary, on which the roughness height and spacing are small compared with the incident wavelength, generates an airborne surface wave which spreads cylindrically but attenuates exponentially both away from and along the surface[1]. Surface waves of this kind have been observed in laboratory experiments over rectangular grooves at ultrasonic frequencies[2], and, at audio-frequencies, over lattices[3,4], regularly spaced parallel cylinders[5], triangular wedges[6,7], square and rectangular strips[7,8]. Audio-frequency measurements outdoors have indicated airborne surface waves over regularly spaced, parallel rows of bricks[9,10]. Surface waves have been detected in both frequency and time domains.

Point-to-point propagation near a surface can be represented by the excess attenuation (EA) spectrum defined by,

$$EA = 20\log\left(\frac{P_{total}}{P_{direct}}\right) \quad (1)$$

where P_{total} is the total pressure and P_{direct} is the direct field pressure at the receiver. Over a smooth acoustically hard ground the excess attenuation spectrum has a maximum magnitude of +6 dB which represents pressure doubling. Effectively, a hard boundary which is rough has a finite impedance and can create a 'soft' ground effect similar to that associated with a porous ground surface. The resulting dip in the EA spectrum is the result of destructive interference between the direct wave and the specular component of the reflected wave. This occurs at a lower frequency over a rough hard surface than over a smooth hard non-porous surface. When a roughness-induced surface wave is generated, the maximum exceeds +6 dB over a frequency range around the frequency of the main surface wave energy. In the time domain the surface wave appears as a wave train following the direct and specularly-reflected wave arrivals. Point-to-point propagation over rough boundaries has been predicted numerically using the Boundary Element Method (BEM) either by full meshing of the surface or via an effective impedance[11]. As the roughness size increases compared with incident wavelengths, so does the incoherent scatter. Moreover, if the roughness spacing is regular, there are diffraction grating effects[7,10].

This paper reports laboratory measurements of EA spectra for regular and random strip arrangements and the influence of increasing receiver height on the surface wave magnitude in both frequency and time domains. Also reported are numerical investigations, of finite array effects, and the influences of quarter wavelength resonances in gaps and grooves. A modal theory[12,13,14] is used to predict propagation over grooves with multiple depths and to offer an explanation for the beat patterns in BEM predictions of spatial distributions of total pressure over periodic arrangements of parallel, identical rectangular strips and grooves.

2 SURFACE WAVE, ARRAY SIZE AND DIFFRACTION EFFECTS

Figure 1 compares EA spectra from anechoic laboratory measurements[10] using a maximum length sequence (MLS) broadband pulse over surfaces composed of 15 parallel identical strips with triangular cross sections on a glass sheet either randomly or regularly spaced with (mean) centre-to-centre spacing of 0.05 m. The curve for random placement is the average of EA spectra measured

over five random distributions. Regular spacing enhances the surface wave near 1.8 kHz and causes a narrowing and deepening of the first roughness-induced destructive interference between the direct and reflected waves which appears as a broader dip in the average of the EA spectra measured over five random arrangements. The first order Bragg diffraction near 3.5 kHz coincides with the low frequency part of the first roughness-induced EA dip. The 2nd order Bragg diffraction at about 7 kHz is responsible for the narrow second dip whereas both the data for regular spacing and the averaged data for five random arrangements show a shallow 2nd order roughness-induced dip in the EA spectrum near 10 kHz.

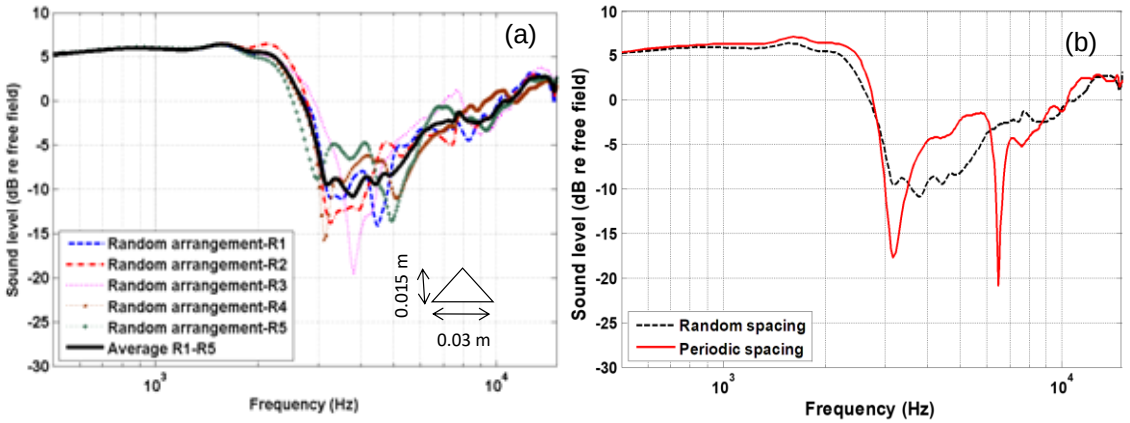

Figure 1. EA spectra measured[10] with source and receiver at 0.07 m height separated by 0.7 m over an array of 15 triangular cross section strips on a glass sheet with a mean centre-to-centre spacing of 0.05 m (a) with five random arrangements and the average of these spectra (b) for uniform (periodic) spacing and the average spectrum for random distributions.

Figures 2(a) and (b) compare EA spectra and waveforms measured as the receiver height is increased by 0.01 m intervals between 0.04 m and 0.12 m. The EA spectra were obtained using a broadband MLS signal and the waveforms were obtained using a Ricker pulse[8]. Increasing the receiver height decreases the peak in the EA spectra near 1.8 kHz due to the surface wave, moves the first roughness-induced destructive interference dip in the EA spectra to lower frequencies and causes it to become deeper. The frequency range of the second order roughness-induced destructive interference is not altered but it becomes shallower. The oscillatory tail after 0.009 s is due to the roughness-induced surface wave and its amplitude decreases as the receiver height increases. The oscillatory tail in Fig. 2(b) has a period of 0.00055 s corresponding to a frequency of 1.8 kHz which is the frequency of the first maxima in the EA spectra in Fig.2(a) and is the frequency of the main surface wave energy.

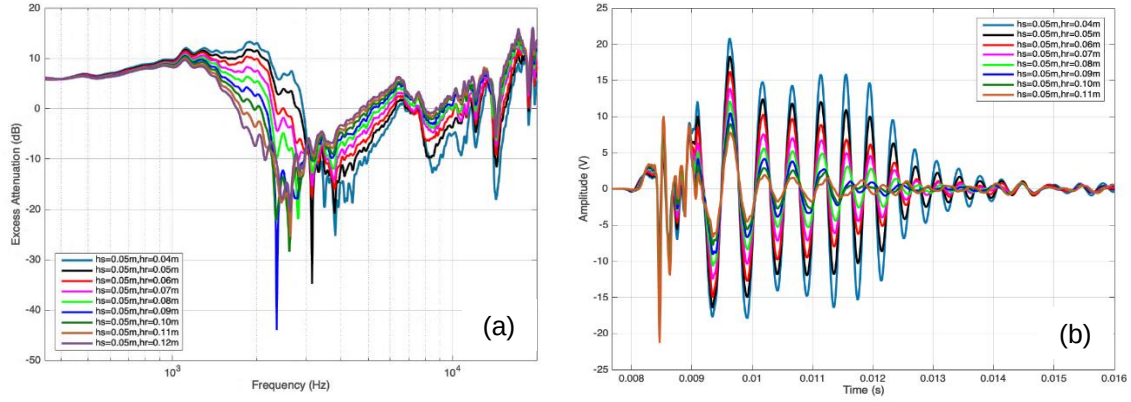

Figure 2. (a) Measured excess attenuation spectra and (b) waveforms for increasing receiver heights between 0.04 m and 0.12 m above 30 x 0.0253 m-high, 0.0126 m thick vertical aluminium strips placed on MDF at a regular edge-to-edge spacing of 0.015 m.

Figure 3 shows a laboratory arrangement of 30 aluminium strips on a comparatively acoustically hard base of medium density fibreboard (MDF) with a point source at a height of 0.07 m above the base and a receiver at a horizontal distance of 0.7 m from the source. To reduce the influence of reflections from the ends of the aluminium strips, strips of felt have been placed along the array edges parallel to the source-receiver axis. Figure 4 compares measurements and Boundary Element Method (BEM) predictions of EA spectra with source and receiver at heights of 0.05 m and 0.04 m respectively above the MDF base and 0.7 m apart over this array without and with felt along the edges[8].

Figure 3. A laboratory arrangement of an array of 30 × 1 m long parallel aluminium strips (height 0.025 m, width 0.0122 m, edge-to-edge separation 0.015 m) on Medium Density Fibreboard (MDF). Strips of felt are placed along the edges of the array parallel to the source-receiver axis.

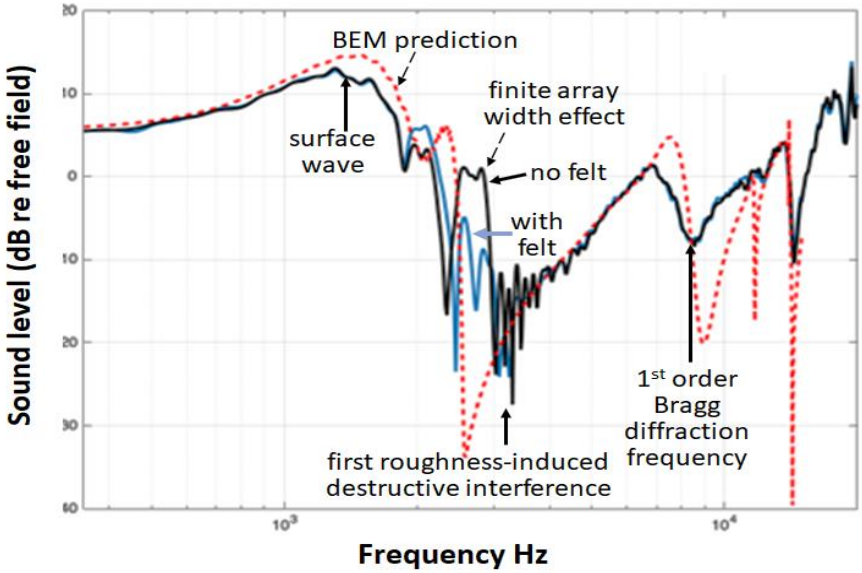

Figure 4. EA spectra measured and predicted by BEM with 0.05 m high source and 0.04 m high receiver separated by 0.7 m over an array of 30 identical parallel rectangular (0.025 m × 0.0122 m) strips regularly spaced at an edge to edge spacing of 0.015 m on MDF without and with felt along the edges parallel to the source-receiver axis.

The peak near 2.5 kHz in the measured EA spectrum without the felt at the edges of the strip array is much reduced if the felt strips are present, which suggests that it results from reflections at the ends of the strips. The surface wave peak in the EA spectrum near 1.6 kHz and the peaks and dips at frequencies higher than 3 kHz are not affected by adding the felt. Moreover, the effect of the finite length of the aluminium strips does not appear in 2D BEM predictions which assume that they are infinitely long.

If the gap width a between parallel rectangular strips of width w is much smaller than incident wavelengths, then the effective impedance of the array surface is that due to a hard-backed porous layer in which the pores are vertical slits (tortuosity = 1) and with porosity Ω and flow resistivity, R_s, given by[7,8,10]

$$\Omega = \frac{a}{a+w},\ R_s = \frac{12\mu}{\Omega a^2}\,. \tag{2}$$

Figure 5 compares EA spectra predicted using the hard backed vertical slit pore layer surface impedance and a BEM simulation for a fully discretized 2D array of 23 parallel identical rectangular (0.025 m × 0.0122 m) strips with edge to edge spacing of 0.0534 m. While both predictions show a roughness-induced surface wave at about 1.2 kHz, the BEM simulation shows additional peaks and dips at higher frequencies.

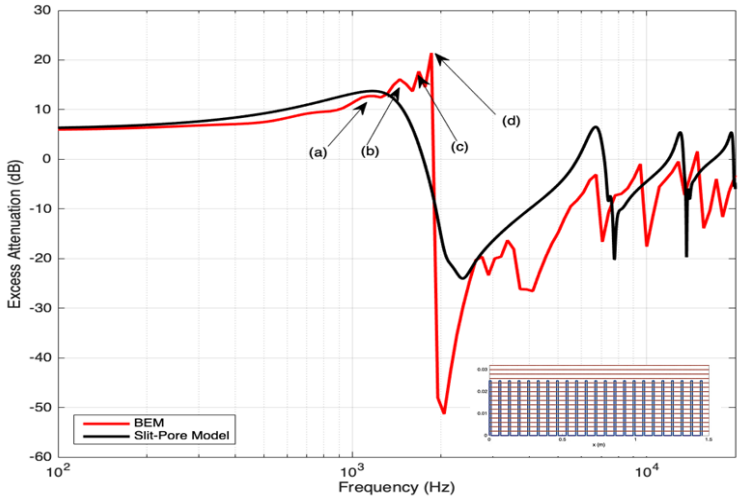

Figure 5. The EA spectrum predicted by the slit pore model for 23 parallel identical rectangular strips separated by 0.0534 m (see inset) compared with that predicted using BEM with full discretization of the surface. The assumed source-receiver geometry is the same as for Fig.4.

3 QUARTER WAVE RESONANCES

Total pressure contour plots for the frequencies corresponding to the arrows in Figure 5 predicted by BEM with full discretization of the surface are shown in Figure 6. A line source is assumed to be at 0.05 m height above the base and 0.01 m to the left of the plotted regions.

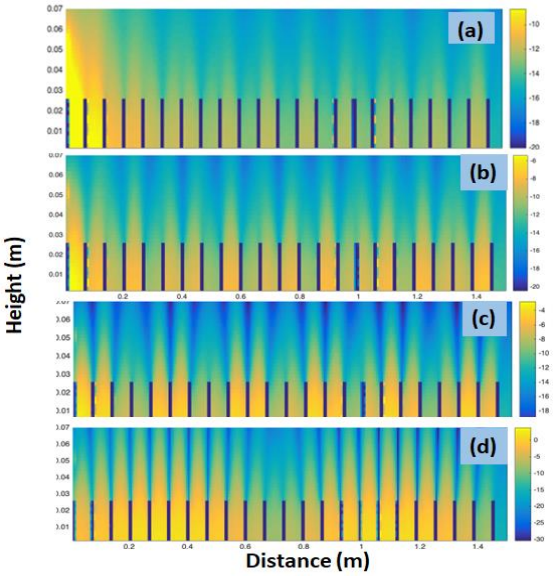

Figure 6. BEM-predicted plots of the total pressure field over 23 periodically-spaced strips at (a) 1.132 kHz (b) 1.45 kHz, (c) 1.68 kHz, and (d) 1.86 kHz [8].

The spectra (see Fig.5) predicted by both BEM calculations and the slit pore model have a peak at 1.132 kHz. The corresponding predicted pressure map (Fig. 6(a)) shows weak resonances in the gaps between strips contributing to surface wave generation. Stronger gap resonances are predicted at 1.45 kHz (Fig. 6(b)), 1.68 kHz (Fig.6(c)) and 1.86 kHz (Fig. 6(d)), which are, respectively, the frequencies corresponding to the second, third and fourth peaks in the BEM-predicted EA spectrum.

The influences of gaps between regularly-spaced identical parallel acoustically hard strips and of uniformly-spaced identical rectangular grooves with the same depth on a hard surface on point-to-point propagation are similar. The impedance at the aperture to each gap between roughness elements or groove entrance dominates the effective impedance of a periodically rough surface. When the height of the gap or depth of groove is an odd multiple of one quarter of the incident wavelength ($\lambda/4$) the phase shift between downward and upward pressure components is π, so there is pressure cancelling at the aperture and significant energy is trapped in the gap. The $\lambda/4$ resonances are modified by end effects at the apertures. Using a modal model to predict the effective surface impedance, which depends on the angle of incidence, for parallel identical grooves, it is found that the frequencies of the minima in the spectrum of the magnitude of the effective impedance are related to the depth of the grooves and thereby in turn to the maxima in the EA spectrum for point-to-point propagation above the groove surface[14].

This is investigated further by considering predictions for a periodically grooved surface where the period consists of two grooves with different depths, (see Figure 7)[14,15]. The corresponding effective surface impedance has been predicted for a pitch of 0.05 m, a groove width of 0.04 m, and groove depths of 0.09 m and 0.06 m. and used in the classical model for point-to-point propagation over an impedance plane to give the EA spectrum shown in Figure 7 for source and receiver at 0.03 m height and separated by 2 m. As well as the surface wave peak near 700 Hz in the predicted EA spectrum, there is peak near 1 kHz greater than +6 dB suggesting the possibility of an additional surface wave.

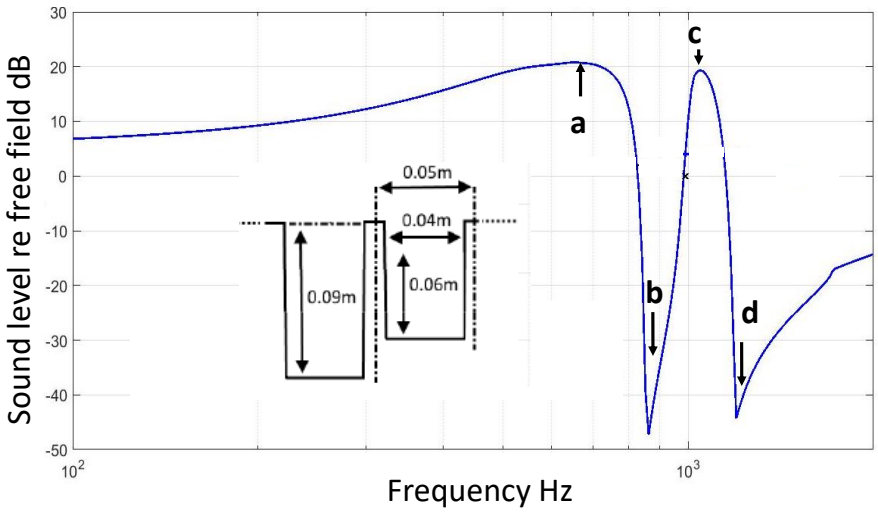

Figure 7. EA spectrum for source and receiver at a height of 0.03 m and separated by 2 m over a periodic variable depth grooved surface each period of which has the two-groove form shown with pitch 0.05 m, gap width 0.04 m, groove depths of 0.09 m and 0.06 m, predicted using the effective surface impedance calculated using the modal model[15].

Figure 8 shows total pressure contours calculated using BEM for a periodically-grooved surface, each period of which is composed of the two grooves shown in Figure 7 for the frequencies labelled **a** to **d** on Figure 7. At 700 Hz the total pressure map, merging of resonances in all the grooves creates a surface wave such that the resonances in the deeper grooves are dominant. At 1030 Hz again the groove resonances combine to create a surface wave at this higher frequency for which the resonances in the shallower grooves are dominant. The regions of relatively low total pressure in the

contours predicted at 860 Hz and 1200 Hz are consistent with the destructive interference dips in the EA spectrum (see Figure 7).

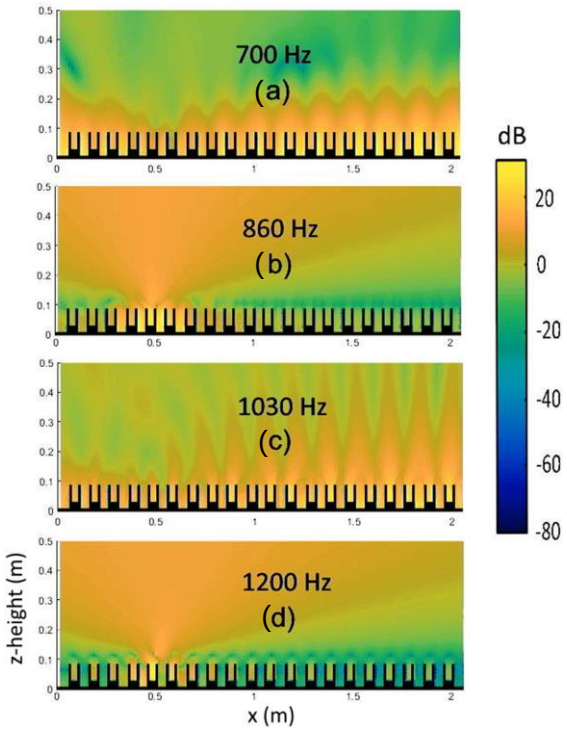

Figure 8. Total pressure plots above the periodic two-groove surface corresponding to Figure 7 predicted by BEM at frequencies of (a) 700 Hz, (b) 860 Hz, (c) 1030 Hz and (d) 1260 Hz corresponding to those labelled accordingly on the EA spectrum in Figure 7. A point source is assumed to be located at x = 0.5 m and 0.03 m above the top of the grooves.

4 BEAT PATTERNS

The patterns in the total pressure maps (Fig.6) at 1.45 kHz, 1.68 kHz and 1.86 kHz indicate some form of beats. Usually, beats result from superposition of waves with different frequencies but, since the pressure contour plots are at specified frequencies, these beats involve the superposition of waves of the same frequency travelling at different speeds. Figures 9(a) and (b) are plots of absolute pressure amplitudes (blue lines) and speeds of surface wave modes (brown lines) predicted by modal theory at two of the frequencies corresponding to peaks labelled (c) and (d) in Fig.5 for groove array dimensions equivalent to the strip array used for the BEM predictions.

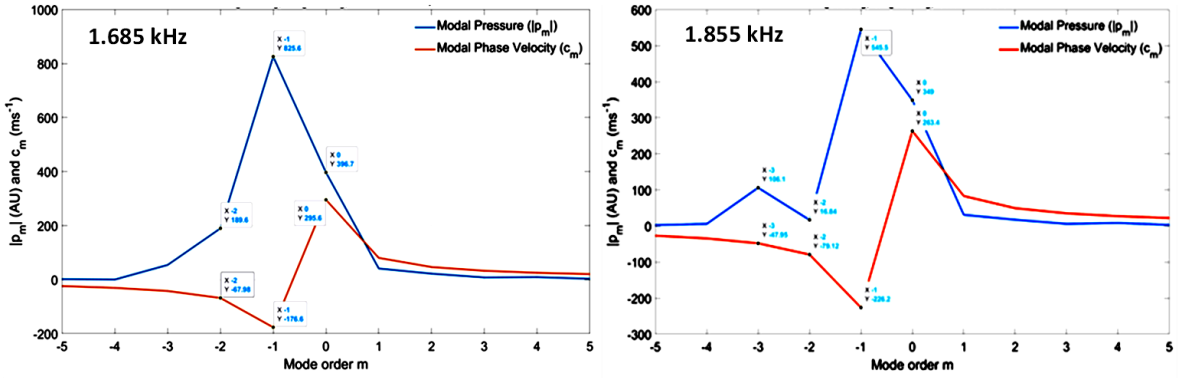

Figure 9. Connected line plots of absolute pressure and phase speed of surface wave modes at 1.685 kHz and 1.855 kHz predicted by modal theory.

The phase speeds of modes with mode number m = 0 are 296 m s^{-1} at 1.685 kHz and 263 m s^{-1} at 1.855 kHz. These modes correspond to the roughness-induced propagating surface wave and the speeds are consistent with slit pore model predictions[16]. However, the plots show larger amplitude modal components with mode number m = −1, having (negative) phase speeds of 177 m s^{-1} at 1. 685 kHz and 226 m s^{-1} at 1.855 kHz. These modes are not self-sustaining but are induced locally within the array to satisfy the non-homogeneous boundary conditions. This suggests that combinations of the propagating and non-propagating modes with mode numbers m = 0 and m = −1 are primarily responsible for the beat patterns.

Figure 10 shows the modal model predictions of the absolute pressure due to combined surface wave modes at 1.685 kHz and 1.857kHz respectively. These are equivalent to Figs. 5(c) and (d) except that the BEM predictions are for regularly-spaced strips rather than grooves, and the BEM predictions are of total pressure including direct and reflected waves, whereas the modal model predictions include only the surface wave modes. Moreover, the modal model assumes that the array is infinite, so the predicted patterns are spatially independent. Consequently, the x-axis for the 1.86 kHz pattern has been adjusted in time to better align the BEM and modal model predictions.

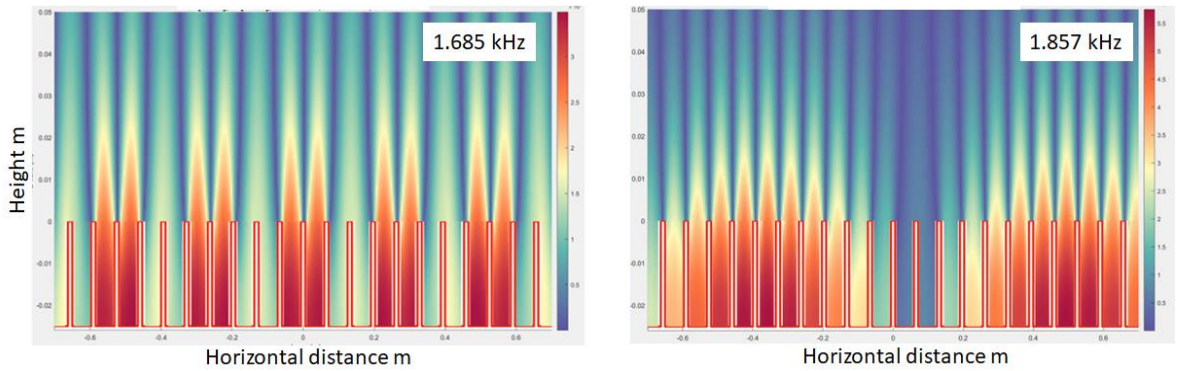

Figure 10. Modal model predictions of absolute pressure due to surface wave components at 1.685 kHz and 1.857 kHz showing beat patterns similar to those in the BEM-predicted total pressure maps in Figs. 6 (c) and (d).

Although surface wave induced by the grooves under broadband excitation from a point source have narrow band spectra rather than being monochromatic, support for the modal model explanation of the beat patterns is provided by Figure 11 which shows the results of adding two plane sinusoidal waves with the same frequency, but with magnitudes and speeds predicted by the modal model for the m = 0 and m = −1 modes at 1685 Hz and 1855 Hz.

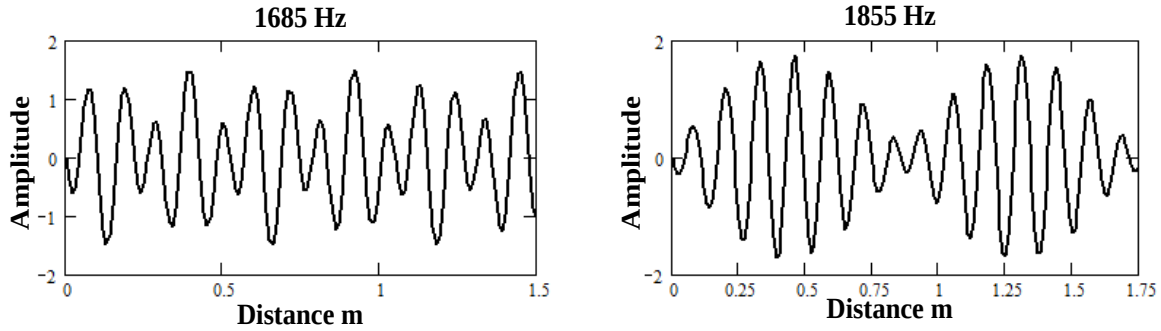

Figure 11. The predicted results of adding plane sinusoidal waves with the relative amplitudes and phase speeds predicted by the modal model at 1685 Hz and 1855 Hz.

5 CONCLUSIONS

Several aspects of point-to-point propagation over periodic rough surfaces have been investigated through laboratory measurements and numerical simulations. Surfaces composed from regularly spaced parallel identical acoustically hard strips on an acoustically hard plane, with strip dimensions and spacing small compared with the shortest wavelength of interest, give rise to surface waves of greater strength than surfaces formed with randomly spaced strips with the same height and mean spacing. Other effects studied include those due to the finite size of the array of roughness elements, quarter wavelength resonances in gaps and grooves and Bragg diffraction. Peaks in the EA spectra above regularly spaced strips or grooves are associated with gap or groove resonances. Periodic arrays of grooves with different depths are predicted to result in multiple surface waves corresponding to quarter wave resonances at each of the depths. BEM predictions of pressure maps above periodically spaced identical parallel rectangular strips show beat patterns. For an equivalent groove array the modal model predicts that these result from superposition of roughness-generated propagating and locally induced non-propagating surface modes.

6 REFERENCES

1. I. Tolstoy. 'Smoothed boundary conditions, coherent low-frequency scatter, and boundary modes' J. Acoust. Soc. Am. 75 1–22, (1984).
2. L. Kelders, J. Allard, and W. Lauriks. 'Ultrasonic surface waves above rectangular groove gratings' J. Acoust. Soc. Am. 103 2030–2033 (1998).
3. R. J. Donato. 'Model experiments on surface waves', J. Acoust. Soc. Am. 63, 700–703, (1978).
4. G. A. Daigle, M. R. Stinson and D. I. Havelock. 'Experiments on surface waves over a model impedance plane using acoustical pulses' J. Acoust. Soc. Am. 99 1993–2005 (1996)
5. D. Berry, S. Taherzadeh and K. Attenborough. 'Acoustic Surface Wave Generation over Rigid Cylinder Arrays on a Rigid Plane' J. Acoust. Soc. Am. 146 2137–2144 (2019)
6. H. Medwin, G. L. D. Spain, E. Childs and S. J. Hollis. 'Low-frequency grazing propagation over periodic steep-sloped rigid roughness elements' J. Acoust. Soc. Am. 76 1174–1190, (1984).
7. I. Bashir, S. Taherzadeh, and K. Attenborough. 'Surface waves over periodically spaced strips' J. Acoust. Soc. Am. 134 4691–4697 (2013).
8. A. Stronach, *An investigation of the sound field above periodically spaced roughness*, PhD Thesis, Open University (2019).
9. L. A. M. van der Heijden. and M. J. M. Martens. 'Traffic noise reduction by means of surface wave exclusion above parallel grooves in the roadside' Appl. Acoust. 15 329–339 (1982).
10. I. Bashir, *Acoustical exploitation of rough, mixed impedance and porous surfaces outdoors*, PhD Thesis, Open University (2014).
11. K. Attenborough, and T. Van Renterghem. Predicting Outdoor Sound 2nd edition, CRC Press, Abingdon, UK, (2021).
12. S. Mellish, S. Taherzadeh and K. Attenborough. 'Approximate impedance models for point-to-point sound propagation over acoustically hard ground containing rectangular grooves' J. Acoust. Soc. Am.147 74–84 (2020).
13. S. Mellish, S. Taherzadeh and K. Attenborough. 'Use of a modal model in predicting the propagation of sound from a point source over a grooved surface' Quart. J. Mech. Appl. Math. 73 367–382 (2021).
14. S. Mellish, S. Taherzadeh and K. Attenborough, 'Audio-frequency surface waves over multiple width and depth grooves', Proc. Internoise22, Glasgow (2022).
15. S. Mellish, S. Taherzadeh and K. Attenborough. 'Modal model prediction of surface waves and resonant characteristics of rectangular grooved gratings' J. Acoust. Soc. Am. 153 2932–2943 (2023).
16. S. Taherzadeh and K. Attenborough. 'Acoustic surface waves above porous and periodic surfaces' Acoustics 2023, Winchester, Proc. IOA Vol.45 Pt. 3 2023.